High Power Laser Science and Engineering, (2023), Vol. 11, e72, 6 pages.
doi:10.1017/hpl.2023.67

HIGH POWER LASER SCIENCE AND ENGINEERING

RESEARCH ARTICLE

High-power free-running single-longitudinal-mode diamond Raman laser enabled by suppressing parasitic stimulated Brillouin scattering

Yuxuan Liu[1,2], Chengjie Zhu[1,2], Yuxiang Sun[1], Richard P. Mildren[3], Zhenxu Bai[4], Baitao Zhang[5], Weibiao Chen[1,2], Dijun Chen[1,2], Muye Li[1], Xuezong Yang[1,5], and Yan Feng[1,2]

[1] *Hangzhou Institute for Advanced Study, University of Chinese Academy of Sciences, Hangzhou, China*

[2] *Shanghai Institute of Optics and Fine Mechanics, Chinese Academy of Sciences, Shanghai, China*

[3] *MQ Photonics Research Centre, School of Mathematical and Physical Sciences, Macquarie University, Sydney, Australia*

[4] *Center for Advanced Laser Technology, Hebei University of Technology, Tianjin, China*

[5] *State Key Laboratory of Crystal Materials, Shandong University, Jinan, China*

(Received 9 June 2023; revised 24 July 2023; accepted 4 August 2023)

Abstract

A continuous-wave (CW) single-longitudinal-mode (SLM) Raman laser at 1240 nm with power of up to 20.6 W was demonstrated in a free-running diamond Raman oscillator without any axial-mode selection elements. The SLM operation was achieved due to the spatial-hole-burning free nature of Raman gain and was maintained at the highest available pump power by suppressing the parasitic stimulated Brillouin scattering (SBS). A folded-cavity design was employed for reducing the perturbing effect of resonances at the pump frequency. At a pump power of 69 W, the maximum Stokes output reached 20.6 W, corresponding to a 30% optical-to-optical conversion efficiency from 1064 to 1240 nm. The result shows that parasitic SBS is the main physical process disturbing the SLM operation of Raman oscillator at higher power. In addition, for the first time, the spectral linewidth of a CW SLM diamond Raman laser was resolved using the long-delayed self-heterodyne interferometric method, which is 105 kHz at 20 W.

Keywords: delay self-heterodyning; diamond Raman laser; linewidth; single-longitudinal mode; stimulated Brillouin scattering

1. Introduction

Wavelength flexible narrow-linewidth single-frequency lasers, credited to the precise wavelength and towering coherence, are valuable for a variety of applications, including laser sensing, quantum technology, coherent detection and astronomical observation[1–5]. Lasers based on the $\chi^{(3)}$ nonlinear gain of the stimulated Raman scattering (SRS) are an effective way to expand the wavelength range of single-frequency lasers as well as a path to acquire high output power[6–14]. This is achieved without consideration of the stringent phase matching conditions integral to efficient $\chi^{(2)}$ interactions, such as optical parametric oscillation, second harmonic generation and sum frequency generation. The typical Raman frequency of materials (10–40 THz) provides wavelength shifts of up to approximately 200 nm in the near-infrared that are 1000 times larger than by stimulated Brillouin scattering (SBS)[15,16]. In tandem with tunable pump lasers, such as Yb fiber lasers, Raman lasers provide an interesting approach to single-frequency lasers across the spectrum.

For SRS actions, a fundamental advantage for generating a single-longitudinal mode (SLM) is that the mode destabilizing effects of the spatial hole burning are avoided since there is no population inversion and therefore no stored energy in the gain material[14,17,18]. In contrast, SLM stability is severely impeded by spatial hole burning for inversion lasers[19], which is caused by the spatial modulation of the inverting particle population consumption. As a result, SLM operation is achieved in simple standing-wave Raman cavities and well above the threshold. Saturation of the gain on neighboring modes occurs due to depletion of the pump, which occurs homogenously over the pump spectrum provided the fundamental pump linewidth is much narrower than the Raman linewidth. In this case, parametric interactions between the pump and the damped phonons allow funneling of the energy of a broadened pump spectrum into a Stokes SLM.

Correspondence to: Xuezong Yang and Muye Li, Hangzhou Institute for Advanced Study, University of Chinese Academy of Sciences, Hangzhou 310024, China. Emails: xuezong.yang@ucas.ac.cn (X. Yang); Muye.li@ucas.ac.cn (M. Li)

Based on these characteristics, SLM Raman lasers with standing-wave cavities have been investigated in both continuous-wave (CW) and pulsed laser outputs[1,11,13,14,17,18,20–23]. Among these, diamond Raman lasers (DRLs) are promising for simultaneously generating SLM output and power scaling due to the remarkable stimulated scattering and thermal properties of diamond[24]. Lux *et al.*[18] reported the first SLM DRL, which comprised a diamond crystal in a linear standing-wave cavity and generated 4 W of SLM Stokes output at 1240 nm. The laser was multimode for higher powers, which was attributed to mode destabilization via strong coupling between the laser power and the cavity length. SLM stabilization techniques, such as intracavity volume Bragg grating[1], cavity locking[20] and introducing nonlinear loss[13,23,25], have been used to improve the SLM diamond Stokes output power. A maximum Stokes power of 20 W at 1178 nm in a linear standing-wave resonator was demonstrated recently[13] by using an intracavity $\chi^{(2)}$ crystal to increase mode competition[26]. However, power limits for intrinsic SLM stability have not been fully tested and are not yet well understood. In addition, the spectral linewidth of CW SLM DRLs has not been resolved below the standard limit (~MHz) of the scanning Fabry–Pérot interferometer (FPI) measurements used in previous works so far.

In this paper, we show that an external V-shaped standing-wave resonator enables SLM diamond Stokes power to be substantially increased up to 20.6 W without the use of intracavity elements. Here, stable SLM operation was achieved due to the elimination of intracavity pump resonance in a V-shaped cavity design, and because of the suppression of parasitic SBS by using cavity-length and spatial-mode selections. The result suggests that parasitic SBS is the leading physical process that destabilizes the SLM operation of a Raman oscillator at high power. At the 20 W level, a linewidth of 105 kHz was measured using the delayed self-heterodyne interferometric (DSHI) technique. The Stokes power stability and SLM frequency stability over periods of up to 60 minutes were also investigated.

2. Experimental setup

The configuration of the DRL is illustrated in Figure 1. An SLM DFB seed laser at 1064 nm and a home-made narrow-band Yb fiber amplifier were utilized as the pump source with a CW output power of up to 70 W and beam quality M^2 of 1.15. Two free-space isolators with thermal lens compensation were employed to provide over 45 dB extinction ratio for protecting the fiber amplifier from the back-reflected beam. A telescope system (L1 and L2) and a plane-convex focus lens (L3, $f = 75$ mm) were utilized to adjust the pump beam size and realize the mode match between the pump and Stokes beams in the diamond crystal. A half-wave plate (HWP) was used to adjust the polarization direction of the pump parallel to the <111> axis of the diamond for accessing the maximum Raman gain. The diamond Raman resonator was designed as a V-shaped standing-wave structure that comprised two plane-concave mirrors (50 mm (M1) and 100 mm (M2) radius of curvature) and a plane mirror (M3). The M1 mirror was coated with highly transmitting material (high transmittance HT > 91.3%) at 1064 nm and highly reflective material (high reflectance HR > 99.9%) at 1240 nm. The M2 mirror, with the coatings of HR > 98.4% at 1064 nm and 0.73% transmittance at 1240 nm, was used as the Stokes output coupler (OC). The M3 mirror was with HR > 99.8% at 1240 nm. M1 was rotated about 12° from the pump optical path to separate the pump and Raman beams, which was similar to Ref. [27]. The Raman medium was a 7 mm × 2 mm × 2 mm chemical vapor deposition (CVD)-grown single-crystal diamond (Type IIa, Element Six) with anti-reflective coatings both at 1064 and 1240 nm and cut for propagation along the <110> direction. The diamond crystal was placed at the focus of the resonator and its temperature was stabilized at 20°C by

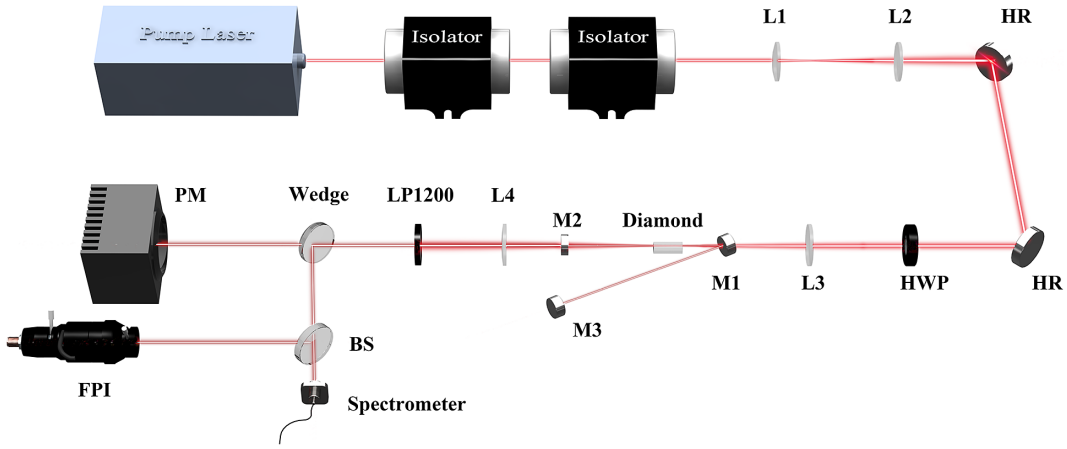

Figure 1. Schematic of the free-running SLM diamond Raman laser. HR, high reflectivity mirror; HWP, half-wave plate; LP1200, long-pass filter cut at 1200 nm; BS, beam splitter; PM, power meter; FPI, scanning Fabry–Pérot interferometer.

using a water-cooled copper holder. The beam waist radii of the pump and Stokes light in the diamond were 15 and 31 μm, respectively. The separation distance from M1 to M2 was 131.1 mm and from M1 to M3 was about 144 mm, which could be tuned by precisely moving the mirror of M3.

3. Results and discussion

The Stokes output power reached the threshold when the pump power increased to 31.5 W. Figure 2(a) plots the Stokes output power and the residual pump power as a function of the injected pump power. The Stokes output power was measured after a long-pass filter cut at 1200 nm (LP1200) and a beam wedge splitter (83.3% transmission), taking into account the losses through the filter and splitter, as shown in Figure 1. The backward residual pump was ejected from the polarization beam splitter in the second isolator (right). As depicted in Figure 2(a), the maximum Stokes output power reached 20.6 W at the pump power of 69 W, corresponding to a slope efficiency of 51.3% and a conversion efficiency of 30% from the pump to the Stokes. After the Stokes threshold, the residual pump power was depleted, indicating a good mode matching between the pump and Stokes beams. The inset shows the Stokes TEM_{00} beam profile at the maximum power, which is a little elliptical due to the astigmatism caused by the angular positioning of M1. At the maximum Stokes power, the Stokes output tended to operate in multiple-longitudinal modes and was accompanied by the SBS spectrum.

Parasitic SBS with higher-order spatial modes was observed prevalently in a V-shape-folded standing-wave diamond Raman resonator[23,28] due to the compensation by the Gouy phase. Compared with a two-mirror quasi-concentric cavity, the V-shaped cavity usually operates away from the stability limit and the higher-order SBS spatial modes are widely spread across the cavity free-spectral range (FSR) due to the non-multiple π Gouy phase. In addition, the astigmatism induced by the T and S plane asymmetry in the V cavity breaks up the degeneracy of Gouy phase and thus no higher-order spatial modes are degenerated. The parasitic SBS was converted from the narrow-linewidth Raman laser, which could result in Raman power depletion and SLM instability. Approaches including the intracavity etalon[28], aperture[23] and nonlinear mode loss methods[13] were proposed to suppress the parasitic higher-order SBS spatial modes. In our case, to diminish the SBS gain and suppress higher-order spatial SBS oscillation, the cavity length was delicately adjusted by tuning M3 and simultaneously the intracavity pump–Raman interaction region was moved to the edge of the diamond crystal, which could be regarded as an aperture for higher modes. Only very narrow cavity length gaps are able to suppress the higher-order spatial SBS, as shown in Figure 7 in Ref. [23]. Here, the cavity-length-related output spectra and longitudinal-mode structures were investigated by using a spectrum analyzer (AQ6370D, Yokogawa, Inc.) and a scanning FPI (Thorlabs, SA210-8B). As demonstrated in Figure 3(a), when the cavity optical length was fixed at 282.17 mm, the central wavelength of the SRS was 1239.6 nm and the spectrum profile showed a typical SLM output. Its SLM FPI trace is shown in Figure 3(b). When the cavity length was precisely increased and decreased by only 14 μm, the spectrum was as illustrated in Figures 3(c) and 3(e), respectively. A satellite peak at a separation of about 70 GHz appeared on the longer wavelength side of the SRS, which matched the theoretical diamond Brillouin frequency shift reported previously[29–31]. At that time, the FPI trace was as shown in Figures 3(d) and 3(f), respectively, and the longitudinal structure was tuned to multiple-longitudinal modes. Here the SBS modes are basically lower-order spatial modes, because higher-order modes have larger beam sizes that are easily blocked by the edge of the diamond crystal. We speculate that the parasitic SBS mainly prompts the multiple-longitudinal-mode operation in SLM DRLs. Therefore, the suppression

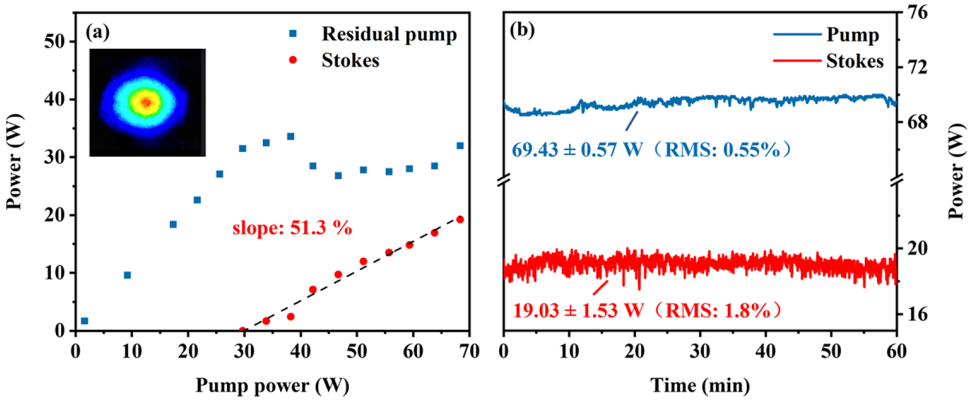

Figure 2. (a) The powers of the Stokes output (red spot) and residual pump (blue square) as a function of pump power. The inset is the Stokes beam profile at the maximum output power. (b) Long-term power stability of pump and Stokes output for 1 hour.

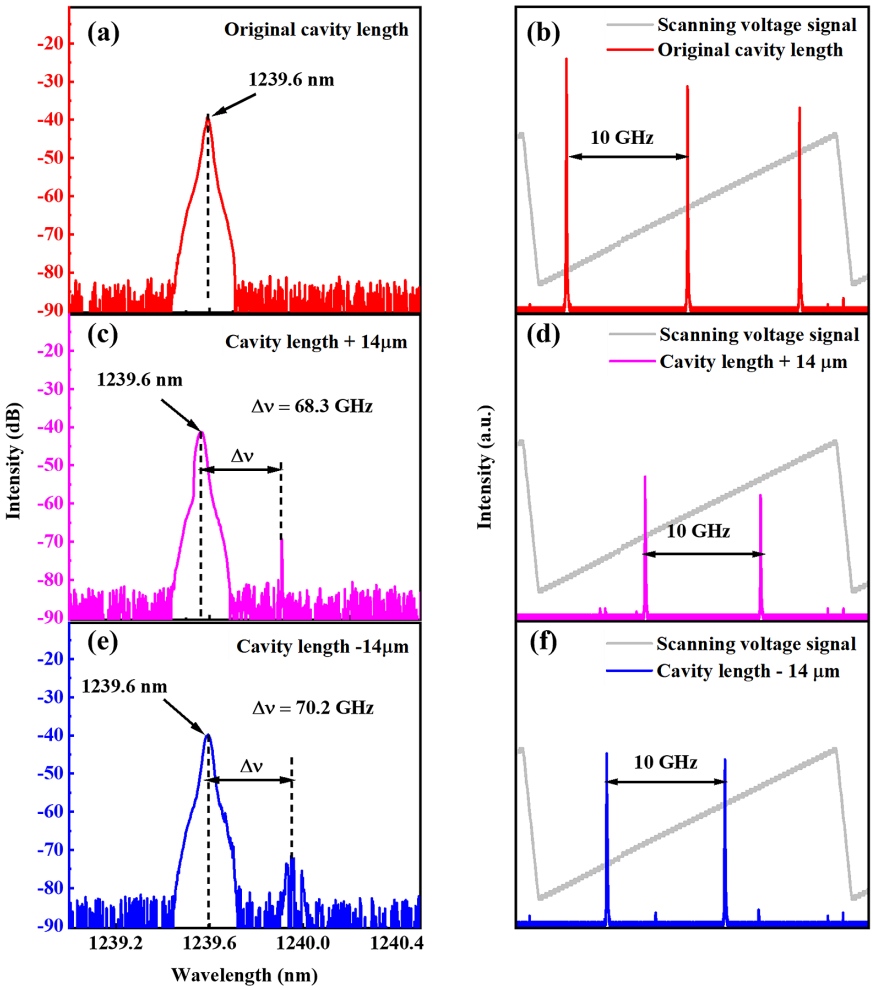

Figure 3. (a), (c), (e) Plots of the spectral characteristics of Stokes outputs for different cavity lengths. (b), (d), (f) Plots of the FPI trace of Stokes outputs for different cavity lengths corresponding to (a), (c) and (e), respectively.

of SBS plays an important role in acquiring stable SLM operation.

As investigated in Ref. [27], a V-shaped oscillator architecture with higher transmissivity at the pump wavelength can provide Stokes output with excellent performance in terms of power stability and conversion efficiency compared to a two-mirror linear oscillator architecture, due to the negligible pump resonance and the insensitive cavity misalignment. Here, M1 was highly transmitting at the pump wavelength and the effective reflectivity was only 0.76% for a cavity round-trip, resulting in a weak intracavity pump and Stokes intensity modulation. The long-term maximum power stability of the incident pump and output Stokes for up to 1 hour are plotted in Figure 2(b). The average pump power and Stokes power were 69.43 and 19.03 W, respectively, and the power root mean square (RMS) values for 1 hour of the pump and Stokes outputs were 0.55% and 1.8%, respectively. Note that the power stability was measured after the thermal steady state of the laser system (about 20 minutes after startup). Although the pump power RMS was 0.2% in Ref. [27], 2.75 times smaller than that in this case, the Stokes power RMS was 2.4% in Ref. [27], compared to 1.8% in this case. The better Stokes power stability here was mainly attributed to the elimination of the Stokes longitudinal-mode beating and the SBS-induced power fluctuations.

The SLM spectral linewidths of the pump and Stokes outputs at the maximum powers were investigated by using the DSHI technique[32,33]. The DSHI measurement system consisted of an acoustic-optical modulator with frequency shift of 150 MHz and a 23-km-long delayed fiber that is able to access an accurate measurement with a minimum linewidth of 50 kHz[34]. An InGaAs photodetector (Newport, 1611FC-AC) and a signal analyzer (Keysight, N9010B) were utilized to analyze the spectral linewidth. Figures 4(a) and 4(b) depict the linewidths of the pump and Stokes outputs, and the measured result and the Lorentzian fitting are plotted as gray squares and red solid lines, respectively. The scanning span, the resolution bandwidth and the video bandwidth of the spectrum analyzer were set as 10 MHz, 51 kHz and 5.1 kHz, respectively. Thus, the effective integration time and sweep time were about 0.02 and 39 ms, respectively. The measured self-heterodyne lineshape results (after the

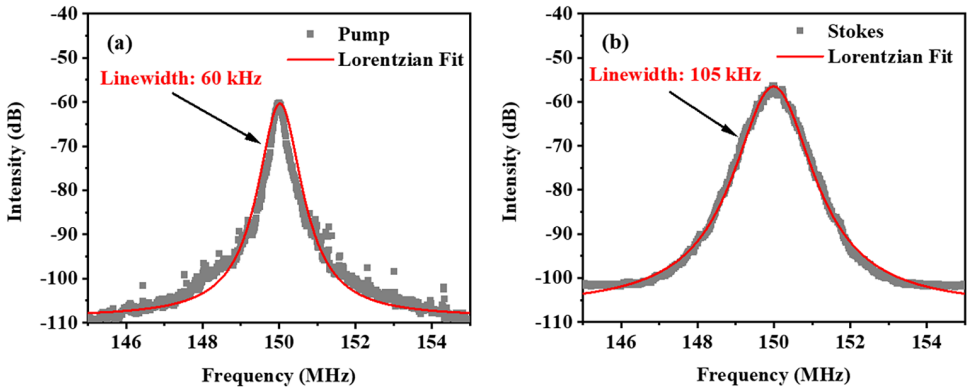

Figure 4. The linewidth of (a) pump and (b) Stokes outputs in the free-running V-shaped DRL. The red solid lines represent Lorentzian fits to the experimental data.

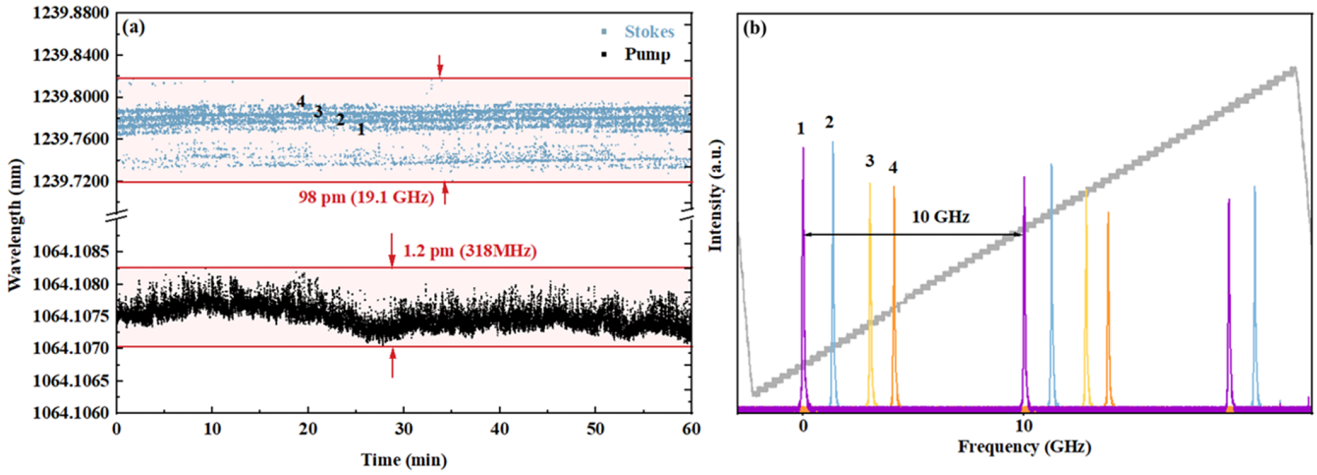

Figure 5. (a) Wavelength stability of the Stokes and pump outputs for 1 hour. (b) Four typical FPI traces of the SLM Stokes output after multiple acquisitions.

average of 100 times) were fitted using a Lorentzian profile and the spectral linewidth was the self-heterodyne linewidth 20-dB down divided by $2\sqrt{99}$[35,36]. Thus, the linewidths of the pump and Stokes outputs were 60 and 105 kHz, respectively, as shown in Figures 4(a) and 4(b). To the best of our knowledge, this is the first demonstration of the linewidth measurement of a CW SLM DRL.

In order to investigate the frequency stability of the free-running SLM DRL, a wavemeter (HighFiness, WS6-200) with an absolute accuracy of 200 MHz was employed. The total cavity optical length of a round-trip was about 564.33 mm, corresponding to a cavity FSR of about 531.6 MHz. The wavelength fluctuations for a period of 1 hour of the SLM Stokes and pump outputs at the maximum power were recorded and are shown in Figure 5(a). The pump wavelength (black) fluctuated within a range of 318 MHz, which complies with the normal frequency drift for commercial SLM DFB lasers. The SLM Stokes wavelength (blue) behaved with obvious mode hopping and jittering due to the free-running cavity, which was susceptible to temperature variation and ambient vibration. There are four pronounced traces (named 1–4) with the starting central wavelengths of 1239.769, 1239.777, 1239.786 and 1239.791 nm, respectively, of which the adjacent frequency interval corresponds to about two or three times the cavity FSR. This indicates that mode hops tend to occur with multiple cavity FSRs. We hypothesize that this is caused by an intracavity parasitic etalon effect between diamond surfaces or other optics surfaces. The majority of Stokes wavelength fluctuation for up to 1 hour was from 1239.720 to 1239.818 nm, which indicated a maximum mode hopping spacing of 19.1 GHz (~36 FSR). A scanning FPI with the FSR of 10 GHz and resolution of 67 MHz was used to further investigate the SLM mode hopping. Figure 5(b) depicts the FPI transmission traces of the SLM Stokes output captured after multiple acquisitions. It was found that four FPI transmission peaks appeared most frequently, and their positions were relatively stable within the same scanning voltage range. The intervals between the four peaks are 1.4, 1.76 and 1 GHz, respectively, which coincide well with the Stokes central wavelength intervals measured using a wavemeter shown in Figure 5(a). In addition, as shown in Figure 5(a), all the wavelength traces exhibit a tendency to drift towards longer wavelengths over time. For

example, trace number 3 started at 1239.777 nm and drifted to 1239.791 nm after 1 hour with frequency variation of about 2.73 GHz. We speculate that the slow wavelength drifting results from the Raman phonon frequency shift caused by the slow temperature decrease of diamond[14,37].

4. Conclusion

A free-running single-frequency external DRL with power of up to 20 W and linewidth of 105 kHz was investigated. The parasitic SBS was suppressed by accurately adjusting the cavity length and using a diamond edge as an aperture, resulting in an SLM SRS operation with great robustness. One-hour wavelength stability with SLM operation was recorded and mode-hopping was observed, which was probably caused by the temperature instability of diamond and cavity length variation. The results strongly confirm the inherent SLM advantages of DRLs and indicate that a simple standing-wave diamond oscillator is able to provide a high-power SLM laser with a compact system.

Acknowledgements

This work was supported by the National Natural Science Foundation of China (No. 62005073); the Program of the State Key Laboratory of Crystal Materials (No. KF2101); the National Key Research and Development Program of China (No. 2020YFC2200300); the Program of the State Key Laboratory of Quantum Optics and Quantum Optics Devices (No. KF202207); the Research Funds of Hangzhou Institute for Advanced Study (No. 2022ZZ01006); and the Hangzhou Agricultural and Social Development initiative Design Project (No. 2022ZDSJ0846).

References

1. O. Lux, S. Sarang, R. J. Williams, A. McKay, and R. P. Mildren, Opt. Express **24**, 27812 (2016).
2. X. Yang, O. Kitzler, D. J. Spence, Z. Bai, Y. Feng, and R. P. Mildren, Opt. Lett. **45**, 1898 (2020).
3. X. Yang, L. Zhang, S. Cui, T. Fan, J. Dong, and Y. Feng, Opt. Lett. **42**, 4351 (2017).
4. J. E. Curtis, B. A. Koss, and D. G. Grier, Opt. Commun. **207**, 169 (2002).
5. D. J. Wineland and W. M. Itano, Phys. Rev. A **20**, 1521 (1979).
6. L. S. Meng, P. A. Roos, and J. L. Carlsten, Opt. Lett. **27**, 1226 (2002).
7. H. Rong, R. Jones, A. Liu, O. Cohen, D. Hak, A. Fang, and M. Paniccia, Nature **433**, 725 (2005).
8. J. Shi, S. Alam, and M. Ibsen, Opt. Express **20**, 5082 (2012).
9. C. Y. Lee, C. C. Chang, P. H. Tuan, C. Y. Cho, K. F. Huang, and Y. F. Chen, Opt. Lett. **40**, 1996 (2015).
10. S. M. Spuler and S. D. Mayor, Appl. Opt. **46**, 2990 (2007).
11. Q. Sheng, R. Li, A. J. Lee, D. J. Spence, and H. M. Pask, Opt. Express **27**, 8540 (2019).
12. O. Kitzler, J. Lin, H. M. Pask, R. P. Mildren, S. C. Webster, N. Hempler, G. P. A. Malcolm, and D. J. Spence, Opt. Lett. **42**, 1229 (2017).
13. Y. Sun, M. Li, R. P. Mildren, Z. Bai, H. Zhang, J. Lu, Y. Feng, and X. Yang, Appl. Phys. Lett. **121**, 141104 (2022).
14. E. Granados, G. Stoikos, D. T. Echarri, K. Chrysalidis, V. N. Fedosseev, C. Granados, V. Leask, B. A. Marsh, and R. P. Mildren, Appl. Phys. Lett. **120**, 151101 (2022).
15. D. Jin, Z. Bai, Z. Lu, R. Fan, Z. Zhao, X. Yang, Y. Wang, and R. P. Mildren, Opt. Lett. **47**, 5360 (2022).
16. Y. Tao, M. Jiang, L. Liu, C. Li, P. Zhou, and Z. Jiang, Opt. Lett. **47**, 1742 (2022).
17. E. Granados, C. Granados, R. Ahmed, K. Chrysalidis, V. N. Fedosseev, B. A. Marsh, S. G. Wilkins, R. P. Mildren, and D. J. Spence, Optica **9**, 317 (2022).
18. O. Lux, S. Sarang, O. Kitzler, D. J. Spence, and R. P. Mildren, Optica **3**, 876 (2016).
19. C. L. Tang, H. Statz, and G. DeMars, J. Appl. Phys. **34**, 2289 (1963).
20. S. Sarang, O. Kitzler, O. Lux, Z. Bai, R. J. Williams, D. J. Spence, and R. P. Mildren, OSA Contin. **2**, 1028 (2019).
21. H. Ma, X. Wei, H. Zhao, M. Zhang, H. Zhou, S. Zhu, H. Yin, Z. Li, Z. Chen, Y. Shen, N. Zong, S. Zhang, and S. Dai, Opt. Lett. **47**, 2210 (2022).
22. Z. Liu, S. Men, Z. Cong, Z. Qin, X. Zhang, and H. Zhang, Laser Phys. **28**, 045002 (2018).
23. M. Li, X. Yang, Y. Sun, H. Jiang, R. P. Mildren, O. Kitzler, D. J. Spence, and Y. Feng, Opt. Express **31**, 8622 (2023).
24. R. P. Mildren, in *Optical Engineering of Diamond* (John Wiley & Sons, 2013), p. 1.
25. X. Yang, O. Kitzler, D. J. Spence, R. J. Williams, Z. Bai, S. Sarang, L. Zhang, Y. Feng, and R. P. Mildren, Opt. Lett. **44**, 839 (2019).
26. K. I. Martin, W. A. Clarkson, and D. C. Hanna, Opt. Lett. **22**, 375 (1997).
27. Y. Sun, M. Li, O. Kitzler, R. P. Mildren, Z. Bai, H. Zhang, J. Lu, Y. Feng, and X. Yang, Laser Phys. Lett. **19**, 125001 (2022).
28. M. Heinzig, T. Schreiber, G. P. Vega, T. Walbaum, and A. Tünnermann, Proc. SPIE **PC12405**, PC124050I (2023).
29. H. Chen, Z. Bai, Y. Cai, X. Yang, J. Ding, Y. Qi, B. Yan, Y. Li, Y. Wang, Z. Lu, and R. P. Mildren, Appl. Phys. Lett. **122**, 092202 (2023).
30. H. Chen, Z. Bai, X. Yang, J. Ding, Y. Qi, B. Yan, Y. Wang, Z. Lu, and R. P. Mildren, Appl. Phys. Lett. **120**, 181103 (2022).
31. R. J. Williams, J. Nold, M. Strecker, O. Kitzler, A. McKay, T. Schreiber, and R. P. Mildren, Laser Photonics Rev. **9**, 405 (2015).
32. T. Okoshi, K. Kikuchi, and A. Nakayama, Electron. Lett. **16**, 630 (1980).
33. Z. Bai, Z. Zhao, Y. Qi, J. Ding, S. Li, X. Yan, Y. Wang, and Z. Lu, Front. Phys. **9**, 768165 (2021).
34. L. Richter, H. Mandelberg, M. Kruger, and P. McGrath, IEEE J. Quantum Electron. **22**, 2070 (1986).
35. L. B. Mercer, J. Light. Technol. **9**, 485 (1991).
36. M. Chen, Z. Meng, J. Wang, and W. Chen, Opt. Express **23**, 6803 (2015).
37. J. B. Cui, K. Amtmann, J. Ristein, and L. Ley, J. Appl. Phys. **83**, 7929 (1998).